Flux Closure Structures in Cobalt Rings

S. P. Li, D. Peyrade, M. Natali, A. Lebib, and Y. Chen

Laboratoire de Microstructures et de Microélectronique (CNRS), 196 Avenue H. Ravera, 92225 Bagneux Cedex, France

U. Ebels, L. D. Buda, and K. Ounadjela

Institut de Physique et Chimie des Matériaux de Strasbourg, 23, rue du Loess, F-67037 Strasbourg Cedex, France

Measurements are reported on the magnetization reversal in submicron magnetic rings fabricated by high-resolution electron beam lithography and lift-off from cobalt thin films. For all dimensions investigated, with diameters of 300–800 nm and a thickness of 10–50 nm, the flux closure state is the stable magnetization configuration. However, with increasing diameter and decreasing film thickness a metastable near single domain state can be obtained during the reversal process in an in-plane applied field.

For the implementation of magnetic materials in high density data storage technologies, an optimization of the geometry and size of small magnetic elements is of importance. Generally, for a given material, the geometry determines which kind of magnetization configuration may be present, while the size and lateral extension control the balance between the demagnetization fields and exchange fields and thus the transformation of one magnetization configuration into another. Many investigations have been carried out so far on elements with simple geometries, such as squares [1], disks [2–4], and rectangles with flat or pointed ends [5–7]. The application of such elements requires a reproducible switching mechanism from one cycle to the next and a narrow switching field distribution inside a large array of identical elements. In this respect, rectangular elements are less well suited due to the formation of end domains [7] and the sensitivity of the switching field on the exact sample shape. Furthermore, for circular disks the vortex formation and vortex displacement can lead to an irreproducible switching and thus a broadened switching field distribution [8].

In order to avoid such effects, recently a vertical magnetoresistive random access memory design was proposed based on a ring-shaped magnetic multilayer stack [8]. Such ring-shaped elements have the advantage that a flux closure (FC) structure can be stabilized without the formation of the central vortex, as in a circular disk [8–11], rendering the FC configuration the energetically more favorable state as compared to the single domain (SD) state.

In this Letter, magneto-optic Kerr effect (MOKE) magnetometry and magnetic force microscopy (MFM) imaging combined with 2D and 3D numerical micromagnetic simulations are used to determine the stability range of the flux closure structure of polycrystalline Co rings as a function of film thickness and ring diameter. For all dimensions investigated, it is shown here that the FC state is the energetically lowest state. However, a metastable SD state can be realized at remanence after saturation in an in-plane

applied field. The probability to trap this metastable SD state increases with decreasing film thickness and increasing outer diameter.

A series of ring arrays were fabricated using electron beam lithography and lift-off techniques. First, a thin polymethylmethacrylate resist layer was spun onto thermally oxidized Si substrates. The resist layer was then patterned with a JEOL 5D2U vector scan generator at 50 keV beam energy. After development, a thin film of Co was first deposited by sputtering and subsequently removed from the unexposed parts of the samples in trichloroethylene. For each thickness of 10, 20, 30, 40, and 50 nm, the following rings of outer diameter (d_o)/inner diameter (d_i) were produced (in nm): 300/100, 400/100, 600/200, 700/300, and 800/400. The rings of each type were arranged in an array of 160 μm $\times$ 160 μm size, with a separation equal to d_o. In order to simplify the electron beam lithography and also to make the flux closure configuration visible in the MFM images, all rings have an octagonal rather than a circular shape.

In Figs. 1(a) and 1(b) two typical room temperature MOKE hysteresis loops are shown as a function of an in-plane applied field for rings of different thickness. There are several characteristic features in loop 1(a). Upon coming from positive saturation, the signal decreases abruptly at a positive critical field, reaches an almost constant plateau of width ΔH_{fc}, and then decreases less abruptly into the reversed field direction. As confirmed by MFM imaging, the first abrupt switch corresponds to a transition from a single domain state into a flux closure state. The MFM contrast observed at field values corresponding to positions (i) and (ii) indicated in the loop of Fig. 1(a) is shown in Fig. 2(a) and 2(b). The strong black and white contrast in Fig. 2(a) corresponds to a SD state, whereas the weaker alternating contrast shown in Fig. 2(b) corresponds to the FC state.

The loop in Fig. 1(b) is qualitatively the same as in Fig. 1(a), except that the transition from the SD into the FC
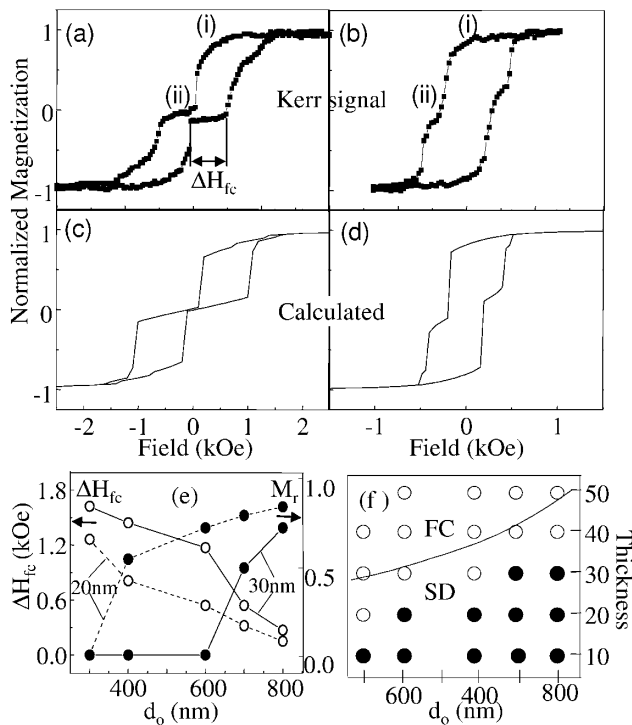
FIG. 1. (a),(b) Typical in-plane MOKE hysteresis loops measured on rings with the same diameters of $d_o = 700$ nm and $d_i = 300$ nm, respectively, but for different thickness of (a) 50 nm and (b) 20 nm. (c),(d) Calculated hysteresis loops for the Co rings as explained in the text. (e) Summary of the experimental remanence ratio M_r (solid circles) and the flux closure plateau width ΔH_{fc} (open circles) as a function of d_o for $t = 30$ nm (solid lines) and $t = 20$ nm (dashed lines). (f) The experimentally determined diagram of the metastable single domain state (solid circles) and the stable flux closure state (open circles). The solid line represents the calculated boundary.

state occurs in a reversed field, yielding a high remanence. At the same time the intermediate plateau at which the flux closure structure is present is much reduced. The loops shown in Figs. 1(c) and 1(d) are obtained from numerical simulation and are discussed later.

The dependence of the remanence ratio M_r and the plateau width ΔH_{fc} on d_o are summarized in Fig. 1(e) for $t = 20$ and 30 nm. Upon increasing the diameter (or decreasing the film thickness), the plateau width decreases and the remanence increases. In Fig. 1(f) a qualitative "phase" diagram is presented as a function of d_o and t, separating the low remanence loops of type 1(a) with positive critical field (open circles) from the high remanence loops of type 1(b) with negative critical field (solid circles).

In contrast to the circular disks described in [3], the remanent SD state is a metastable state. This is demonstrated in Fig. 3 by repeated MFM scans over the same area for rings prepared at remanence after applying a saturating in-plane field. The lift scan height is held at a large distance of 150 nm, which still allows one to visualize the strong dipolar contrast of the SD state, but not the much weaker contrast of the FC state.
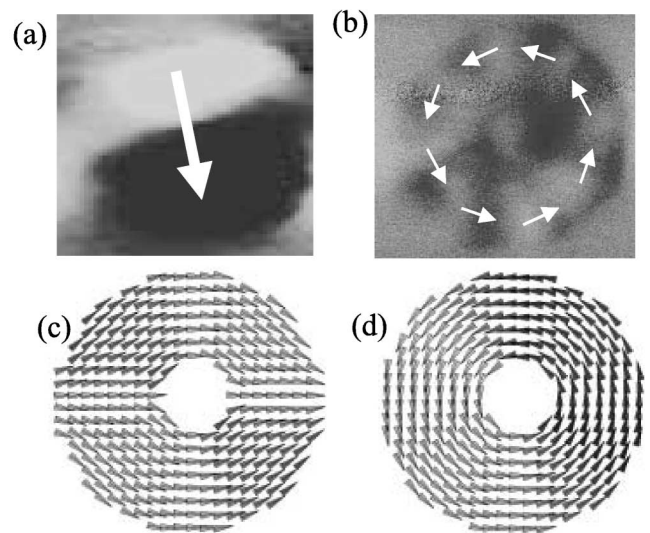

FIG. 2. MFM contrast of octagonal ring elements ($d_o = 800$ nm, $d_i = 400$ nm, and $t = 20$ nm). (a) The strong black and white contrast signifies a single domain state. (b) The weaker contrast with 8 alternating bright and dark segments signifies a FC configuration. (c),(d) The spin configurations of circular ring elements ($d_o = 200$ nm, $d_i = 50$ nm, and $t = 5$ nm) obtained from 3D micromagnetic simulations.

In Fig. 3(a), almost all rings (96%) are in a SD state when the MFM tip is scanned for the first time (from top to bottom). The tip field is strong enough to switch the rings during the scan, as can be seen by the fact that for many rings only the upper black half is visible. Repeating the scan a second time (from bottom to top), only 25% of the rings are found in the SD state. After the fourth scan [from bottom to top, Fig. 3(b)], only 14% of the rings are found in the SD state. It is noted that the reversal of the rings from the SD into the FC state is not a relaxation effect. Changing the scan area, after having "erased" in one area most of the SD states by repeated scanning, the new area shows again the high remanence SD state of Fig. 3(a).

The magnetization reversal of the negative part of the hysteresis loop as studied by MFM is shown in Fig. 4, with the positive saturation field pointing in the upward
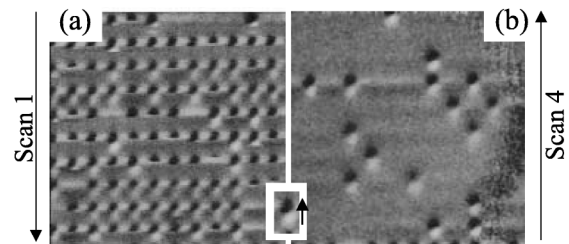

FIG. 3. Repeated MFM images of the same area of 20 μm × 20 μm for rings of $t = 20$ nm and $d_o = 800$ nm at remanence after in-plane saturation. The images were scanned (a) in a first scan from top to bottom and (b) in a fourth scan from bottom to top, at a lift scan height of 150 nm using a Digital Instruments Nanoscope System, Dimension 3100, equipped with standard CoCr tips.
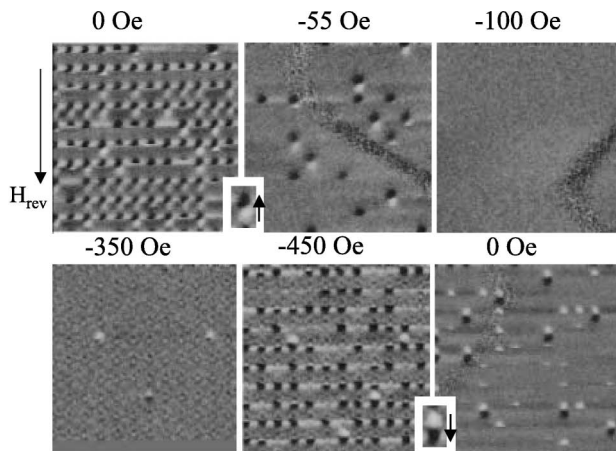
FIG. 4. MFM images of an area of 20 μm $\times$ 20 μm pattern for rings of $t = 20$ nm and $d_o = 800$ nm taken in an applied field and measured at a lift scan height of 200 nm. The arrow indicates the reversed field direction H_{rev} (negative). The field values are noted on top of each image.

direction and the negative reversed field pointing in the downward direction. The MFM images were scanned in the applied reversed field at values indicated on top of each image. In order to minimize the tip-sample interaction, a lift scan height of 200 nm was chosen. The actual field value at each ring is hence the sum of the applied field and the tip field. Starting from the remanent state at 0 Oe (induced in the absence of the tip), a large number of rings switches from the SD into the FC state due to the tip field; see Fig. 3. However, after several scans a number of rings are stable and a finite field of -100 Oe is required to switch all rings from the SD into the FC state. Upon increasing the reversed field value to -350 Oe, three rings can be seen to switch into the reversed SD state. The field range between -100 and -350 Oe hence corresponds approximately to the plateau range ΔH_{fc}; see Fig. 1. At -450 Oe (maximum field of the magnet used) 70% of the rings are in the reversed SD state. Reducing the field back to zero, the remanent state is lower (25%) than the initial remanent state (96%). This is because the initial remanent state was obtained in the absence of the tip field, while the remanent state at the end of the hysteresis cycle is obtained in the presence of the tip field.

The magnetization configuration of the Co rings described in Figs. 1 and 2 was further investigated by 3D numerical micromagnetic modeling. In Figs. 2(c) and 2(d) the SD and FC configurations of circular rings are shown as obtained by minimizing the total free energy of the system [12] using the material parameters of Co [13]. The real system is discretized into $N_x \times N_y \times N_z$ cubic cells of constant magnetization. The mesh size is 2.5 nm, which is smaller than the exchange length of Co (3.37 nm). Starting from a given configuration, the local energy minimum is found by the time integration of the Landau-Lifshitz-Gilbert (LLG) equation [14,15]. The stable state is reached when the maximum value of the torque is smaller than a predetermined tolerance.

For the relatively large system sizes studied here, the 3D meshing would require a too large number of discretization cells. Therefore, in order to investigate qualitatively the evolution of the spin configuration during the in-plane hysteresis cycle, the publicly available 2D code OOMMF [16] was employed from which the same static magnetization configuration for circular rings was obtained as those shown in Figs. 2(c) and 2(d) (same material parameters and ring sizes).

The in-plane hysteresis loops calculated from the 2D code for octagonal rings with dimensions corresponding to those of Figs. 1(a) and 1(b) are shown in Figs. 1(c) and 1(d), respectively. The qualitative shape of the experimental hysteresis loops is well reproduced by the calculation. Furthermore, these calculations confirm that the FC and SD states of Fig. 2 develop during the reversal and that the reversal occurs via the transformation from a SD to a FC state and back into the reversed SD state. From these hysteresis loops, the boundary between the metastable SD and the FC state was determined, using the criterion that the critical field for the transformation of the SD state into the FC state changes sign from positive to negative. The calculated boundary confirms qualitativley the experimental phase diagram of Fig. 1(f).

To understand the size dependence and stability of the FC and SD state of the rings, the energetics of the two configurations need to be considered and compared to the circular disk ($d_i = 0$). Since anisotropy energy is negligible, the zero field magnetization configuration is determined by the balance between the exchange and magnetostatic energy which is controlled by the thickness and diameter of the ring.

For a circular disk, there exists a transition from the FC state into the SD state upon reducing both the disk diameter and the film thickness [3]. In the FC state the energy is dominated by the exchange energy due to the formation of a central vortex. In contrast, the single domain state is dominated by the demagnetization energy produced by the surface charges at the lateral surfaces. Upon decreasing the film thickness at constant diameter, the dipolar energy is reduced and eventually the total energy of the SD state becomes lower than that of the FC state [3,17]. On the other hand, decreasing the disk diameter at constant thickness, the relative contribution of the exchange energy of the central vortex increases and renders the FC state less stable below a critical diameter.

While the energetics of the SD state for the rings and the circular disk are not too different, with the demagnetization energy dominating, it differs for the FC state. The absence of the central vortex reduces the exchange energy substantially in the rings and with this the total energy of the FC structure making the FC the lowest energy state [8]. Hence it is clear that upon reducing the outer diameter of the rings, the transition into a SD domain state, which takes place in circular disks, is suppressed in the ring geometry. For example, the 3D calculations show that for circular disks of $t = 5$ nm the FC state is the energetically lower

state only above a critical diameter of 60 nm. In contrast, for the ring geometry the FC state is always the energetically lower state. The latter can be considered correct only as long as d_i is larger compared to the diameter of the central vortex which forms in circular disks (20 nm for bulk Co [18]).

As shown in the diagram of Fig. 1(f), the probability of the formation of a remanent metastable SD state increases with increasing outer diameter. This dependence on diameter is opposite to the phase boundary of the circular disk [3]. The micromagnetic calculations indicate that for increasing diameter the energy of the SD and FC state both decrease and approach each other. Hence, the probability increases for trapping the SD state in a local energy minimum at in-plane remanence.

From the micromagnetic modeling of the hysteresis loops [Figs. 1(c) and 1(d)] this "trapping" can be accounted for by a local energy minimum of the SD state which is separated from the FC state by an exchange energy barrier. The calculations show that the transition from the SD state to the FC state occurs via the formation of vortexlike perturbations similar to those shown in Ref. [8]. These perturbations increase the exchange energy. For the thicker and smaller rings [Figs. 1(a) and 1(c)] the reduction in magnetostatic energy due to the formation of the FC configuration is large enough to compensate this increase in exchange energy. In this case the FC state can be adopted at remanence without any external energy and a comparatively large external field is required to transform the FC state into the reversed SD state. In contrast, in the thinner and larger rings [Figs. 1(b) and 1(d)], the gain in magnetostatic energy cannot compensate the increase in exchange energy and an external field is required to cross the exchange energy barrier and to adopt the FC state.

In summary, combined MOKE hysteresis loop and MFM studies on submicron Co rings reveal that the complete reversal takes place via the transformation of the saturation SD state at high positive field into a FC state at low field, back into the reversed single domain state at high negative field. The field range ΔH_{fc} over which the intermediate flux closure structure is stable increases with increasing thickness and decreasing diameter. At the same time, the probability of formation of a metastable SD state decreases. Making use of the rotation sense of the flux closure structure for magnetic memory devices, a decrease of the ring diameter stabilizes the flux closure structure; however, for thin rings a metastable single domain state may be reached at remanence.

[1] R. P. Cowburn, A. O. Adeyeye, and M. E. Welland, Phys. Rev. Lett. **81**, 5414 (1998).

[2] M. Hehn, K. Ounadjela, J. Bucher, F. Rousseaux, D. Decanini, B. Bartenlian, and C. Chappert, Science **272**, 1782 (1996).

[3] R. P. Cowburn, D. K. Koltsov, A. O. Adeyeye, M. E. Welland, and D. M. Tricker, Phys. Rev. Lett. **83**, 1042 (1999).

[4] Y. Xu, A. Hirohata, L. Lopez-Diaz, H. T. Leung, M. Tselepi, S. M. Gardiner, W. Y. Lee, J. A. C. Bland, F. Rousseaux, E. Cambril, and H. Launois, J. Appl. Phys. **87**, 7019 (2000).

[5] K. J. Kirk, J. N. Chapman, S. McVitie, P. R. Aitchison, and C. D. W. Wilkinson, Appl. Phys. Lett. **75**, 3683 (1999).

[6] J. Yu, U. Rüdiger, A. D. Kent, L. Thomas, and S. S. P. Parkin, Phys. Rev. B **60**, 7352 (1999).

[7] Y. Zheng and J. Zhu, J. Appl. Phys. **81**, 5471 (1997).

[8] J. Zhu, Y. Zheng, and G. Prinz, J. Appl. Phys. **87**, 6668 (2000).

[9] T. Shinjo, T. Okuno, R. Hassdorf, K. Shigeto, and T. Ono, Science **289**, 930 (2000).

[10] C. Pike and A. Fernandez, J. Appl. Phys. **85**, 6668 (1999).

[11] R. E. Dunin-Borkowski, M. R. McCartney, B. Kardynal, and D. J. Smith, J. Appl. Phys. **84**, 374 (1998).

[12] See, for example, A. Hubert and R. Schäfer, *Magnetic Domains* (Springer-Verlag, Berlin, 1998), p. 148, and references therein.

[13] The material parameters are saturation magnetization $M_s = 1400$ emu/cm^3, exchange constant $A_{ex} = 1.4 \times 10^{-6}$ erg/cm, zero magnetocrystalline anisotropy, and damping parameter $\alpha = 1.0$ which determines the relaxation of the magnetization into its local effective equilibrium field direction [see M. R. Scheinfein and J. L. Blue, J. Appl. Phys. **69**, 7740 (1991)].

[14] Y. Nakatani, N. Uesaka, and N. Hayashi, J. Appl. Phys. **28**, 2485 (1989).

[15] For the evaluation of the stray field the fast Fourier method is implemented. The numerical stability of the time integration of the LLG equation is assured by the use of an implicit forward difference method for the time discretization [14]. Further details will be published elsewhere [L. Buda *et al.,* IEEE Trans. Magn. (to be published)].

[16] A 2D code to calculate the magnetization configuration and its field evolution for 2D flat elements is described on http://math.nist.gov/oommf. This code requires as input the sample shape and dimensions, the material parameters, cell size, and tolerance criterion. All parameters used are the same as in Ref. [13] except the mesh size which is 5 nm.

[17] R. P. Cowburn and M. E. Welland, Appl. Phys. Lett. **72**, 2041 (1998).

[18] J. Miltat, in *Applied Magnetism,* edited by R. Gerber, C. D. Wright, and G. Asti, NATO ASI Series (Kluwer, Dordrecht, 1994).